Friction-induced vibration of a stick–slip oscillator with random field friction modelling

Han Hu, Anas Batou, Huajiang Ouyang

Friction-induced vibration of a stick-slip oscillator with random field friction modelling

Han Hu[a,b], Anas Batou[b,*], Huajiang Ouyang[a]

[a]*Department of Mechanical, Materials and Aerospace Engineering, School of Engineering, University of Liverpool, Liverpool L69 7ZF, United Kingdom*

[b]*MSME, Univ Gustave Eiffel, CNRS UMR 8208, Univ Paris Est Creteil, F-77474 Marne-la-Vallée, France*

Abstract

In this paper, stochastic planar stick-slip motions are investigated using a slider-on-belt model where the coefficient of friction (COF) of the contact interface is modelled as a random field. New three-variable stick-slip transition criteria are proposed to improve the accuracy and robustness of the algorithm. Stochastic analyses are performed concerning the Peak-to-Valley value of the displacement and friction forces and the time duration of the stick state. It is found that the correlation length of the COF random field is dominantly responsible for the stochastic behaviours of the system. In contrast, the belt velocity and the mean value of the COF have a significant influence on the time duration of the stick state compared with the corresponding deterministic slider-on-belt model.

Keywords: stick-slip motion, random field, coefficient of friction, stochastic analysis

1. Introduction

Stick-slip vibrations are frequently encountered in the dynamic response of mechanical systems involving friction. They are self-sustained phenomena induced by dry friction [1] and can bring desired or undesired consequences concerning applied scenarios. For instance, string instruments like cello play melodious music thanks to the stick-slip effect, but squeaky automotive disc brakes [2], chattering machine tools [3], and even earthquakes are also caused by the same origin [4]. Two states characterise the stick-slip motion as its name implies: one stick state where two surfaces in contact have null relative velocity and friction is a constraining force, and one slip state where they have non-zero relative velocity and friction now behaves like an applied force. The non-smooth transition between these two states makes the system exhibits rich nonlinear behaviours, including bifurcation and chaos [1, 5, 6]. As a result, friction-induced stick-slip vibrations have been a continuously active topic for theoretical analysis [7, 8, 9, 10, 11, 12, 13, 14] and industrial applications [15, 16, 17].

Methods to model dry friction are various [18]. The most widely used dry friction model is undoubtedly Coulomb's friction law. However, in recent decades dry friction is recognised to be of stochastic nature from both theoretical [19] and experimental [20, 21] aspects. It is indeed too ideal to treat the coefficient of friction (COF) as an invariant quantity as the contacting objects are generally surrounded by complicated conditions (e.g., contacting surfaces' roughness,

*Corresponding author

Email address: batoua@liverpool.ac.uk (Anas Batou)

contact forces between the objects, and the interfacial temperature). Alternatively, stochastic approaches of modelling friction appear to be a more appropriate choice. Looking into the existing literature, randomness in friction has been taken into consideration through imposing stochastic motion of the contacting objects [22, 23], modelling COF as a random variable [24, 25], random process [26, 27] or random field [28, 29]. In this work, the focus is on planar stick-slip motions, in which the concept of the slider-on-belt model is adopted, that is to say, a rigid body is set on a moving belt, driven by the friction force at the contact interface, with constraining force from the spring connected to a fixed boundary. Different from the classical slider-on-belt model, as shown in Fig.1(a), which is often studied in one dimension, the present work takes into account the spatially distributed randomness in COF to model it as a random field. Indeed, due to the imbalance of momentum caused by uneven friction forces, the rigid body is expected to rotate and move in the transverse direction, too, which makes the problem two-dimensional, as shown in Fig.1 (b). In the authors' previous work [29], the statistical properties of the frictional force and torque were analysed for a rigid body moving on a plane with a constant velocity and random field COF modelling. However, the dynamical planar stick-slip motion under such conditions was not studied. The present paper is meant to bridge this gap and extend that previous work.

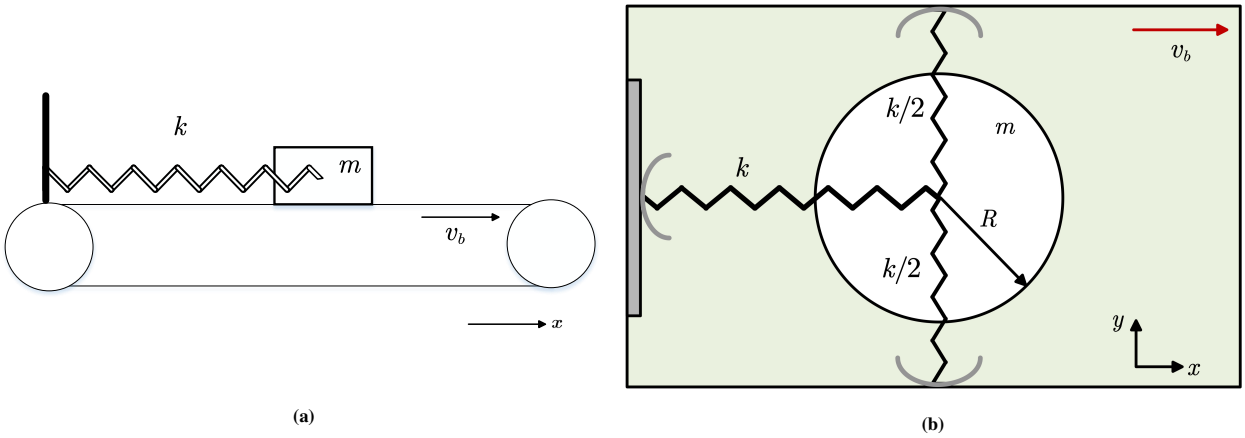

Fig. 1. (a) 1D deterministic slider-on-belt model; (b) 2D stochastic slider-on-belt model.

When dealing with 2D stick-slip problems, numerical difficulties are often encountered, especially near the stick-slip transition points, where the direction and magnitude of friction and relative velocity are not known *a priori* [30]. Therefore, proper stick-slip transition criteria are of crucial importance. Tariku and Rogers [31] proposed force-balance and spring-damper stick-slip algorithms and compared five different models determining the friction force of the stick or slip state in a 2D case. However, none of them concerns the rotation of the moving object. Neither do methods proposed in [32, 33]. Kardan et al. [34] proposed a stick-slip condition for the general motion case based on the concept of *instantaneous centre of zero acceleration*. They considered the rotation of the moving object, but the algorithm is only effective when there is an external torque applying on the object so that the instantaneous centre of zero acceleration is not null. Kudra and Awrejcewicz [35] took into account rotation and developed an event-driven method to capture precisely the stick-slip transition points. The integration of friction force and torque

are approximated by Padé approximants or their modifications for computational efficiency. In a following research, Kudra and Awrejcewicz [36] proposed a new regularised model to approximate general integrations of the friction force, for which the accuracy and robustness of the model are improved.

This paper extends the method described in [35, 36] by taking into account random friction forces and torques to form new general 3D stick-slip criteria in the stochastic setting. The stick-slip transition points are captured with enhanced accuracy by event-driven and bisection methods. This new robust algorithm enables the study of the friction-induced vibration problems in planar motion with a random COF field. Then this paper establishes new results concerning the impact of system parameters, e.g. the correlation length of the COF random field, on some quantities of interest, e.g. the variations of the magnitude of random friction forces and torques. The layout of this paper is outlined as follows: in section 2 the stick-slip oscillator under investigation is introduced as the baseline model. The method used to generate COF random field, the governing equations for the dynamical system, and the proposed stick-slip criteria are also presented. In section 3 stochastic analysis of the stick-slip oscillator is performed concerning quantities of interest with varying parameters. Bifurcation and spectra analyses of the stochastic model are conducted and compared with the deterministic model in section 4. Section 5 concludes and closes the paper.

2. Dynamics of the planar stick-slip oscillator

2.1. Baseline model

In this section, the baseline model is introduced. It consists of a rigid disc of mass m and radius R connected at its centre to a fixed support by a horizontal spring of stiffness k, and to two moving supports by two vertical springs of stiffness $k/2$. The disc is in contact with a belt moving at velocity v_b in the x-direction with friction through its bottom surface, as pictorially depicted in Fig.1(b). The baseline model is different from the classic slider-on-belt model, as shown in Fig.1(a), in such a way that the motion in the transverse direction, as well as rotation, takes place because the spatially distributed randomness of the COF is taken into consideration, which is generally absent for a classic slider-on-belt model. Additionally, the bottom surface of the disc is modelled to be smooth and the belt surface to be rough, which means that the belt surface determines the fluctuations in COF. In dynamical analysis, the static COF μ_s is generally larger than the kinetic one μ_k, and they are distinguished by the application of the Coulomb's friction law, as depicted in Fig.2 where the equation

$$\mu_\mathrm{k} = 0.9\,\mu_\mathrm{s} \tag{1}$$

is satisfied globally for the deterministic (classic) model and locally for the stochastic model, which will be elaborated in the following content.

To take into account its spatial statistical fluctuations, the static COF is modelled as a homogeneous lognormal random field. The COF field, located within the domain Ω_D, is represented by $\{\mathbb{H}_s(\mathbf{x}), \mathbf{x} \in \Omega_D\}$ where $\mathbf{x} = (x, y)$ is the 2D-coordinate in the belt-fixed frame for which the origin is the geometric centre of the belt at the initial position. It should be noted that a homogeneous random field is determined by: (1) the correlation structure; (2) the marginal probability distribution. For the former, a correlation function $\{\mathrm{R}_\mathbb{H}(\mathbf{x}, \mathbf{x}'),\ \mathbf{x}, \mathbf{x}' \in \Omega_D^2\}$ of exponential type, which is a

typical correlation structure in the random field theory [37], is adopted in this paper and is expressed as

$$\mathrm{R}_{\mathbb{H}}(\mathbf{x}, \mathbf{x}') = \mathrm{e}^{-\frac{\|\mathbf{x}-\mathbf{x}'\|^2}{l^2}}, \tag{2}$$

where l is the correlation length. Please note that the exact definition of correlation length should be $l_c = l\sqrt{\pi}/2$, but in this work l will be used to indicate correlation length for the concise representation, and it will not violate the main conclusions of this paper. For the marginal probability distribution, a lognormal distribution is applied to the random variables in the random field. The reasons for the choice of the lognormal distribution, as explained in [29], are: (1) it is near a bell shape as the normal distribution; (2) it is almost surely positive, which is compatible with the concept of COF. The COF random field is modelled as attached to the belt surface. Furthermore, the belt is sufficiently long so that during the simulation the disc will not leave the belt, and the COF random field does not repeat itself, i.e., no periodic boundary condition necessities.

The values of the critical parameters used in the simulation are given in Table.1, where $\mu_{\mathbb{H}_s} = \mathbb{E}[\mathbb{H}_s(\mathbf{x})]$ is the mean value of the static COF random field and $\sigma_{\mathbb{H}_s}$ its standard deviation. The corresponding kinetic COF can be derived through Eq.(1). These parameters will serve as a basis for the stochastic analysis in Sec.3.

Table 1: Parameters used for simulation

Model / Parameter	m [kg]	k [N/m]	v_b [m/s]	R [m]	l [m]	static COF
Deterministic model	10	30	0.2	0.5	/	$\mu_\mathrm{s} = 0.5$
Stochastic model	10	30	0.2	0.5	0.1	$\mu_{\mathbb{H}_s} = 0.5$, $\sigma_{\mathbb{H}_s} = 0.1$

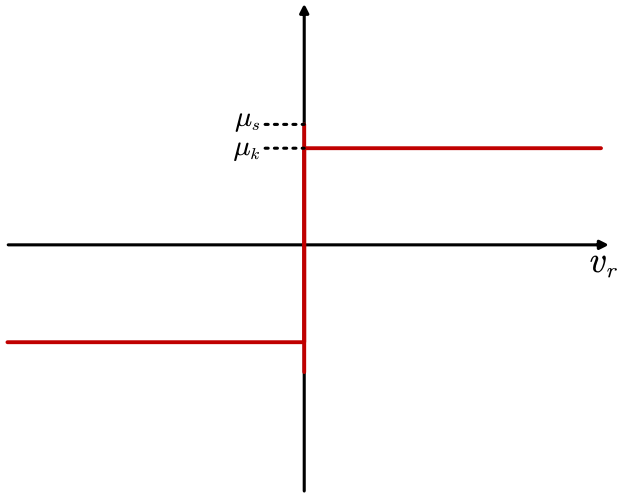

Fig. 2. Coulomb's friction model.

2.2. COF random field generation

In the dynamics regime, a closed-form solution (e.g., displacement) is generally not available due to the nonlinearity induced by the friction model. Therefore, a numerical approach is required to perform simulations. Numerical

methods are versatile for the generation of a random field, e.g., Turning bands method [38, 39], Spectral method [40, 41], Matrix decomposition method [42] and methods based on Karhunen-Loève expansion [43]. For interested readers, please refer to [44] for a comprehensive review of Gaussian random field generation. The differences among these methods mainly concern their algorithm complexity and accuracy. As compared in [44], the Matrix decomposition method is the only method that reflects the correlation structure of the random field exactly but with an algorithm complexity of $O(N^3)$. As a result, the conventional Matrix decomposition method becomes computationally intractable when the number of nodes N is large. The large cost can be alleviated through the circulant embedding method proposed by Dietrich and Newsam [45], which makes use of the block-Toeplitz structure of the covariance matrix of a homogeneous (isotropic) random field, sampled at equispaced node points on a rectangular domain. In such a case, the generation process can be significantly accelerated via the Fast Fourier Transform (FFT) technique, and the algorithm complexity thus declines to $O(N \log N)$.

The generation procedure of a two-dimensional normalised homogeneous Gaussian random field $\mathbf{\Gamma} \sim \mathcal{N}(\mathbf{0}, \mathbf{\Sigma})$, where $\mathbf{\Sigma}$ is the prescribed covariance matrix using the circulant embedding method is presented in Appendix A. For more details, please refer to [45, 46]. The Gaussian random field with prescribed mean value μ and standard deviation σ can be obtained simply by $\hat{\mathbf{\Gamma}} = \mu + \sigma\mathbf{\Gamma}$. The COF random field, which is of lognormal distribution, can be obtained through Nataf transform [47] as $\hat{\mathbb{H}}_s = \mathrm{F}^{-1}[\Phi(\hat{\mathbf{\Gamma}})] = \exp(\hat{\mathbf{\Gamma}})$, where $\Phi(\cdot)$ is the cumulative distribution function (CDF) of the standard normal variable, $\mathrm{F}^{-1}(\cdot)$ is the inverse CDF of the lognormal random variable with specified mean $\mu_{\mathbb{H}}$ and standard deviation $\sigma_{\mathbb{H}_s}$ and $\hat{\mathbb{H}}_s$ is a discretised representation of the random field $\mathbb{H}_s(\mathbf{x})$. It should be noted that the use of Nataf transform will slightly change the prescribed covariance structure. However, this effect is negligible for the coefficient of variation (CV) of the random variable less than 0.3, as being analysed quantitatively in a recent research [48]. In the present case, as indicated in Table.1 $\mathrm{CV}_{\mathbb{H}_s} = 0.2$ and is consistent with the requirement.

Three realisations of COF random field are presented with different correlation length, as shown in Fig.3. Values of random variables apart from the grid points are determined through interpolation.

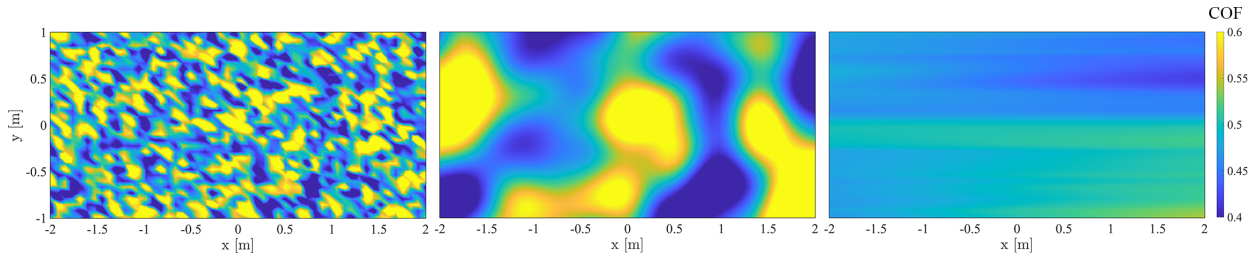

Fig. 3. Random field realisations with correlation length (1) $l/R = 10^{-1}$; (2) $l/R = 10^{0}$; (3) $l/R = 10^{1}$.

2.3. Governing equation of the system

2.3.1. Deterministic system

The governing equation of the deterministic system is introduced first in this section. In this case, the COF is modelled spatially uniform (e.g. constant for the whole contact interface). The problem thus becomes one-dimensional, as

illustrated in Fig.1(a) and can be expressed mathmetically as

$$m\ddot{x} + kx + f_d = 0, \tag{3}$$

where f_d is the friction force represented as

$$f_d = \begin{cases} -kx & \text{Stick} \\ -\mu_k mg & \text{Slip.} \end{cases} \tag{4}$$

Equation (3) is relatively standard for the friction-induced vibration problem and has been extensively investigated in the literature. The stick-slip transition criteria are briefly presented here and can be compared with those of the stochastic system to be presented in the next section: (1) stick to slip when $kx \geq \mu_s mg$; (2) slip to stick when $kx < \mu_s mg$ and $\dot{x}$ becomes zero. The accuracy of capturing the slip to stick transition point can be further improved through the bisection method or interpolation method.

2.3.2. Stochastic system

The governing differential equation of the stochastic system can be expressed as

$$\mathbf{M}\ddot{\mathbf{q}} + \mathbf{K}\mathbf{q} + \mathbf{Q_s} = \mathbf{0}, \tag{5}$$

where $\mathbf{M} = diag([m, m, J])$ is the mass matrix and $J = \frac{1}{2}mR^2$ is the moment of inertia, $\mathbf{K} = diag([k, k, 0])$ is the stiffness matrix. The authors would like to note that for stiffness matrix $\mathbf{K}$ no coupling is assumed between the horizontal and vertical directions. This is for the use of so-called 'idealised' springs: the horizontal and vertical springs go along with the disc in the y- and x-direction, respectively, as has been shown in Fig.1(b). $\mathbf{q} = [x, y, \phi]^{\mathrm{T}}$ is the generalised coordinate vector and $\mathbf{Q_s} = [-F_{sx}, -F_{sy}, -T_s]^{\mathrm{T}}$ is the vector containing two perpendicular friction forces and the torque, which are stochastic (random in time) due to the spatial randomness of the COF and for which the values can be distinct concerning different state of the disc such that for the state of stick

$$F_{sx} = kx,\ F_{sy} = ky,\ T_s = 0, \tag{6}$$

and for the state of slip

$$\begin{aligned} \mathbf{F_s} &= [F_{sx}, F_{sy}]^{\mathrm{T}} = \iint_S P\mathbb{H}_k(\mathbf{x}) \frac{\mathbf{v_p}}{\|\mathbf{v_p}\|} \mathrm{d}S, \\ T_s &= \iint_S P\mathbb{H}_k(\mathbf{x}) \frac{\mathbf{x} \times \mathbf{v_p}}{\|\mathbf{v_p}\|} \mathrm{d}S, \end{aligned} \tag{7}$$

where $\mathbf{v_p} = [\dot{x} - v_b, \dot{y}]^{\mathrm{T}}$, $\mathbb{H}_k(x, y) = 0.9\,\mathbb{H}_s(x, y)$ is the kinetic COF random field, $P = mg/(\pi R^2)$ is the normal pressure that is considered constant in this paper. Then one gets

$$\begin{aligned} F_{sx}(\dot{x}, \dot{y}, \dot{\phi}) &= \iint_S P\mathbb{H}_k(x, y) \frac{\dot{x} - v_b - \dot{\phi}y}{\sqrt{(\dot{x} - v_b - \dot{\phi}y)^2 + (\dot{y} + \dot{\phi}x)^2}} \mathrm{d}S \approx \sum_i P\mathbb{H}_k(x_i, y_i) \frac{\dot{x} - v_b - \dot{\phi}y_i}{\sqrt{(\dot{x} - v_b - \dot{\phi}y_i)^2 + (\dot{y} + \dot{\phi}x_i)^2}} \Delta S_i, \\ F_{sy}(\dot{x}, \dot{y}, \dot{\phi}) &= \iint_S P\mathbb{H}_k(x, y) \frac{\dot{y} + \dot{\phi}x}{\sqrt{(\dot{x} - v_b - \dot{\phi}y)^2 + (\dot{y} + \dot{\phi}x)^2}} \mathrm{d}S \approx \sum_i P\mathbb{H}_k(x_i, y_i) \frac{\dot{y} + \dot{\phi}x_i}{\sqrt{(\dot{x} - v_b - \dot{\phi}y_i)^2 + (\dot{y} + \dot{\phi}x_i)^2}} \Delta S_i, \\ T_s(\dot{x}, \dot{y}, \dot{\phi}) &= \iint_S P\mathbb{H}_k(x, y) \frac{\dot{\phi}(x^2 + y^2) + x\dot{y} - y(\dot{x} - v_b)}{\sqrt{(\dot{x} - v_b - \dot{\phi}y)^2 + (\dot{y} + \dot{\phi}x)^2}} \mathrm{d}S \approx \sum_i P\mathbb{H}_k(x_i, y_i) \frac{\dot{\phi}(x_i^2 + y_i^2) + x_i\dot{y} - y_i(\dot{x} - v_b)}{\sqrt{(\dot{x} - v_b - \dot{\phi}y_i)^2 + (\dot{y} + \dot{\phi}x_i)^2}} \Delta S_i. \end{aligned} \tag{8}$$

In practice, the friction forces and torque should be computed in a discrete way, as shown in the third part of (8), where (x_i, y_i) is the coordinate of the centroid of the i-th discrete area, $\mathbb{H}_k(x_i, y_i)$ is the COF of this centroid and ΔS_i its area. The authors note that in general the contact pressure is not constant due to roughness but the combination of $P\mathbb{H}_k(x, y)$ accounts for the fluctuations in the resultant frictional forces and torque. In this case, an averaging P is taken over the contact interface to justify the random field modelling of COF, as described in [29].

The governing equations show that in stick state the frictional forces and torque of the disc are uncoupled in three dimensions. However, in the slip state, they are coupled due to the components in the friction vector $\mathbf{Q_s}$, as shown in Eq.(8), which causes difficulties in the numerical computation. Consequently, particular care should be taken to capture the occurrence of the state transition, as will be discussed in the next section.

2.4. A three-variable stick-slip transition criteria for the stochastic system

As mentioned in the introduction, the stick-slip transition criteria are crucial in the friction-induced vibration problems involving stick-slip phenomena. In this section, a new three-variable event-driven integration method is proposed to deal with the stick-slip transition, as an extension of [35], in which the algorithm is two-variable. Firstly, nondimensionalising the relevant variables, one gets

$$x^\star = (x - v_b t)/R,\ y^\star = y/R,\ \dot{x}^\star = (\dot{x} - v_b)/(R\omega_n),\ \dot{y}^\star = \dot{y}/(R\omega_n),\ \dot{\phi}^\star = \dot{\phi}/\omega_n,$$

$$P^\star = PR^2/(mg) = 1/\pi,\ \mathrm{d}S^\star = \mathrm{d}S/R^2.$$

It is to be noted that the time derivative is nondimensionalised by $\omega_n = \sqrt{k/m}$ such that $(\dot{\bullet})^\star = (\dot{\bullet})/\omega_n$. Secondly, define a non-dimensional relative velocity magnitude $\lambda = \sqrt{\dot{x}^{\star 2} + \dot{y}^{\star 2} + \dot{\phi}^{\star 2}}$ such that

$$\dot{x}^\star = \lambda\cos\theta\cos\psi,\ \dot{y}^\star = \lambda\cos\theta\sin\psi,\ \dot{\phi}^\star = \lambda\sin\theta. \tag{9}$$

Thirdly, consider a non-dimesionalised triplet $(F^\star_{sx}, F^\star_{sy}, T^\star_s)$ of friction force and torque like in Eq.(8) but in a limit case where the kinetic COF random field is replaced by its static counterpart. The justification of using static COF to model friction is accomplished by the concept of "virtual sliding" [22], which indicates that the disc is actually not sliding on the belt. The triplet depicts the normalised boundary as the limit of the duration of the stick state and can be expressed as

$$\begin{aligned}
F^\star_{sx}(\dot{x}^\star, \dot{y}^\star, \dot{\phi}^\star) &= \iint_{S^\star} P^\star \mathbb{H}_s(x, y) \frac{\dot{x}^\star - \dot{\phi}^\star y^\star}{\sqrt{(\dot{x}^\star - \dot{\phi}^\star y^\star)^2 + (\dot{y}^\star + \dot{\phi}^\star x^\star)^2}} \mathrm{d}S^\star\,, \\
F^\star_{sy}(\dot{x}^\star, \dot{y}^\star, \dot{\phi}^\star) &= \iint_{S^\star} P^\star \mathbb{H}_s(x, y) \frac{\dot{y}^\star + \dot{\phi}^\star x^\star}{\sqrt{(\dot{x}^\star - \dot{\phi}^\star y^\star)^2 + (\dot{y}^\star + \dot{\phi}^\star x^\star)^2}} \mathrm{d}S^\star\,, \\
T^\star_s(\dot{x}^\star, \dot{y}^\star, \dot{\phi}^\star) &= \iint_{S^\star} P^\star \mathbb{H}_s(x, y) \frac{\dot{\phi}^\star(x^{\star 2} + y^{\star 2}) + x^\star \dot{y}^\star - y^\star \dot{x}^\star}{\sqrt{(\dot{x}^\star - \dot{\phi}^\star y^\star)^2 + (\dot{y}^\star + \dot{\phi}^\star x^\star)^2}} \mathrm{d}S^\star.
\end{aligned} \tag{10}$$

Substituting Eq.(9) into Eq.(10), more concise formulations are obtained and can be characterised by the azimuth pair (θ, ψ) as

$$
\begin{aligned}
F_{sx}^{\star}(\theta,\psi) &= \iint_{S^{\star}} P^{\star}\mathbb{H}_s(x,y)\frac{\cos\theta\cos\psi - y^{\star}\sin\theta}{\sqrt{(\cos\theta\cos\psi - y^{\star}\sin\theta)^2 + (\cos\theta\sin\psi + x^{\star}\sin\theta)^2}}\mathrm{d}S^{\star}\,,\\
F_{sy}^{\star}(\theta,\psi) &= \iint_{S^{\star}} P^{\star}\mathbb{H}_s(x,y)\frac{\cos\theta\sin\psi + x^{\star}\sin\theta}{\sqrt{(\cos\theta\cos\psi - y^{\star}\sin\theta)^2 + (\cos\theta\sin\psi + x^{\star}\sin\theta)^2}}\mathrm{d}S^{\star}\,,\\
T_{s}^{\star}(\theta,\psi) &= \iint_{S^{\star}} P^{\star}\mathbb{H}_s(x,y)\frac{(x^{\star 2} + y^{\star 2})\sin\theta + x^{\star}\cos\theta\sin\psi - y^{\star}\cos\theta\cos\psi}{\sqrt{(\cos\theta\cos\psi - y^{\star}\sin\theta)^2 + (\cos\theta\sin\psi + x^{\star}\sin\theta)^2}}\mathrm{d}S^{\star}.
\end{aligned}
\tag{11}
$$

By sampling the azimuth pair (θ, ψ) from the set $D' = [0, 2\pi]^2$, the integrals in Eq.(11) are calculated numerically using their corresponding discretised forms. An ellipsoidal-like domain Ω_l with limit boundary surface Γ_l is thus formed by the collected results, as depicted in Fig.4. The stick-slip transition criteria can be stated as follows.

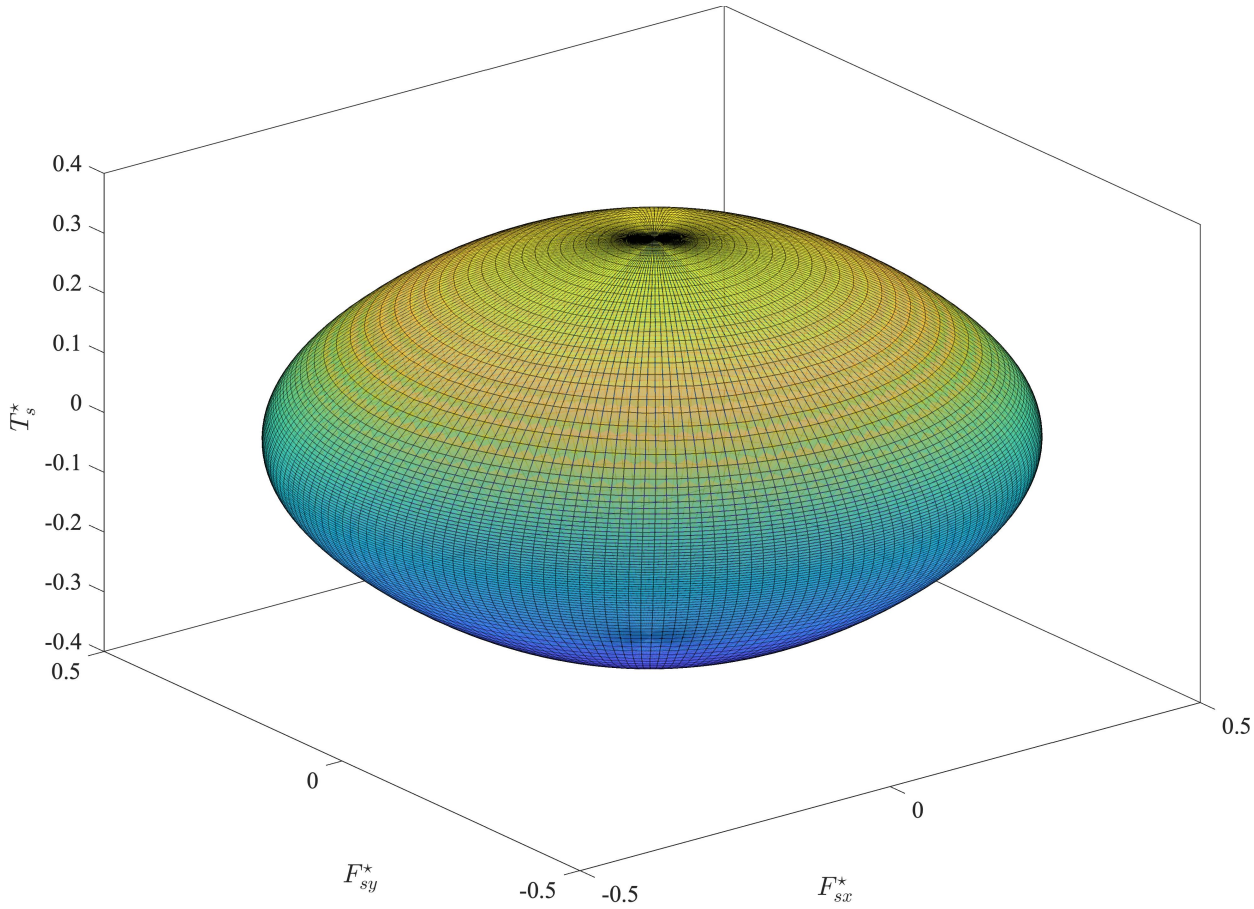

Fig. 4. Limit boundary surface of static friction triplet.

(1) Slip-to-stick criteria. Theoretically, the slip state lasts as long as $\lambda > 0$ and ends only at $\lambda = 0$ and the real non-dimensionalised friction triplet $\mathbf{Q}_s^{r\star} \in \Omega_l \backslash \Gamma_l$. However, since the point satisfying $\dot{x}^{\star} = 0$, $\dot{y}^{\star} = 0$ and $\dot{\theta}^{\star} = 0$ simultaneously is a singular point, a threshold ε_λ is set up and a criterion function $C(\dot{x}^{\star}, \dot{y}^{\star}, \dot{\phi}^{\star}) = \lambda - \varepsilon_\lambda$ is defined such that the slip state remains when $C(\dot{x}^{\star}, \dot{y}^{\star}, \dot{\phi}^{\star}) \geq 0$ and breaks when $C(\dot{x}^{\star}, \dot{y}^{\star}, \dot{\phi}^{\star}) < 0$ and $\mathbf{Q}_s^{r\star} \in \Omega_l \backslash \Gamma_l$. The key to capture the occurrence of the transition point is to continuously detect the sign change of the criterion function

$C(\dot{x}^\star, \dot{y}^\star, \dot{\phi}^\star)$ during the simulation. Bisection method is used to enhance the accuracy of the detection of the transition point [12]. As done in [35], after the detection of the earliest time t_r for which $C(\dot{x}^\star, \dot{y}^\star, \dot{\phi}^\star) < 0$ and the validation of the condition $\mathbf{Q}_s^{r\star} \in \Omega_l \backslash \Gamma_l$, a small velocity jump needs to be applied for the next time step t_r^+ to improve the robustness of the algorithm:

$$\begin{cases} \dot{x}\,(t_r^+) = v_b \\ \dot{y}\,(t_r^+) = 0 \\ \dot{\phi}\,(t_r^+) = 0 \end{cases}, \tag{12}$$

where $\dot{x}\,(t_r^+)$, $\dot{y}\,(t_r^+)$ and $\dot{\phi}\,(t_r^+)$ are the initial velocity terms in the next stick state.

(2) Stick-to-slip criteria. Firstly, the real friction triplet during the stick state as shown in Eq.(6) is nondimensionalised by the normal force $F_N = mg$ and the nominal torque $T_N = F_N R$ as

$$F_{sx}^{r\star} = F_{sx}/F_N,\ F_{sy}^{r\star} = F_{sy}/F_N,\ T_s^{r\star} = T_s/T_N. \tag{13}$$

Then the real non-dimensionalised friction triplet $\mathbf{Q}_s^{r\star} = (F_{sx}^{r\star},\ F_{sy}^{r\star},\ T_s^{r\star})$ is compared against the domain Ω_l. If $\mathbf{Q}_s^{r\star}$ is inside the domain Ω_l, the stick state maintains; if $\mathbf{Q}_s^{r\star}$ is on the boundary Γ_l or outside the domain Ω_l, the stick state then breaks and transits to the next slip state. In the present model, since the frictional torque is always zero during the stick state (as shown in Eq.(6)), the limit boundary surface Γ_l can thus collapse to its equatorial circle, e.g., see Fig5. At the stick state, the disc moves completely following the belt, so displacement only occurs in the x-direction. In the

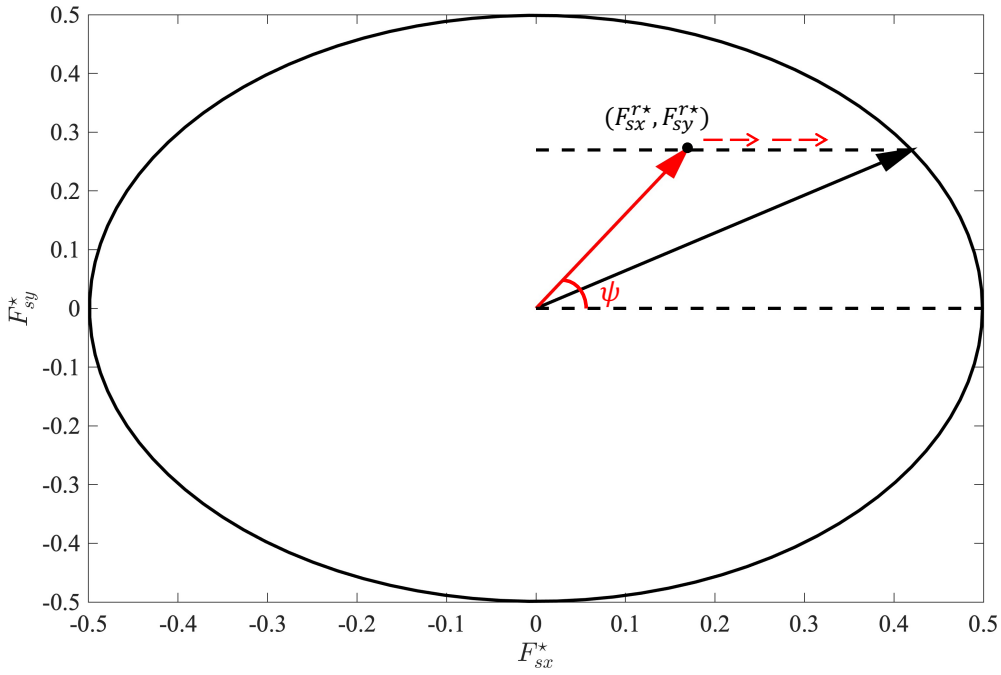

Fig. 5. Equatorial circle of the limit boundary surface.

y-direction, the displacement remains and so does the friction force. Therefore, the current state of the friction pair $(F_{sx}^{r\star}, F_{sy}^{r\star})$ will solely translate horizontally along the way dashed arrows point shown in Fig.5, until it finally reaches

the boundary, breaks the stick state and enters into the next slip state. Consequently, the azimuth angle ψ changes continuously and can be obtained as $\psi = \arctan(F_{sy}^{r\star}/F_{sx}^{r\star})$. Bisection method is again used here to capture a more accurate transition point. After the break of the current stick state, a small velocity jump is applied at the initial time step t_l^+ of the next slip state to the disc as

$$\begin{cases} \dot{x}(t_l^+) = v_b - \varepsilon_\lambda \cos\psi \\ \dot{y}(t_l^+) = -\varepsilon_\lambda \sin\psi \\ \dot{\phi}(t_l^+) = 0 \end{cases} . \tag{14}$$

The velocity jump essentially makes the criterion function $C(\dot{x}^\star, \dot{y}^\star, \dot{\phi}^\star) = 0$ at time step t_l^+ and avoids the oscillation problems that usually take place as a result of the indefinite moving direction when the relative velocity between the disc and belt is minimal. For instance, Fig.6 compares simulation results using the stochastic baseline model with and without velocity jump incorporated in the algorithm. It can be observed from Fig.6(b) that a sudden decrease in the friction force occurs if no velocity jump is applied, which is caused by the fact that the moving direction is not properly dealt with after the release of the state of stick. Consequently, a lag presents in the displacement compared with the results of which that incorporated the velocity jump, as shown in Fig.6(a). Therefore, the robustness of the algorithm can be improved by performing the velocity jump.

The accuracy of the proposed algorithm can be controlled by the threshold parameter ε_λ. If a small threshold ε_λ is chosen, the time step used for simulation should be reduced correspondingly. To quantify the influence of ε_λ, several numerical experiments are conducted using the stochastic baseline model. The result obtained from $\varepsilon_\lambda = 10^{-5}$ is used as a reference. The error can be calculated by using

$$\text{error} = \int_0^T (x(t) - x_{\text{ref}}(t))^2 \, \mathrm{d}t = \sum_i (x_{t_i} - x_{\text{ref},t_i})^2 \Delta t_i, \tag{15}$$

where $x(t)$ and $x_{\text{ref}}(t)$ are respectively the disc's displacement and reference displacement in the x-direction, and x_{t_i} and x_{ref,t_i} are the corresponding discrete values at time t_i, Δt_i is the time step at t_i satisfying $\sum_i \Delta t_i = T = 100$ [s]. The results shown in Fig.7 indicate that the error decreases and the results converge with the decrease of ε_λ.

Finally, the overall algorithm is summarised in a flowchart depicted in Fig.8.

3. Stochastic analysis of the stick-slip oscillator.

In this section, stochastic analysis is performed to investigate the system responses regarding some quantities of interest, which will be introduced first. Then the uncertainties of these quantities with respect to the variation of some system parameters (e.g., the correlation length, the belt velocity, and the mean value of the COF random field) are quantified and compared with the outputs of the deterministic model. The results are reported successively in the following subsections. The objective of this investigation is to assess the impact of the local COF fluctuations on the friction-induced vibration and determine the situations when it is important to take it into account.

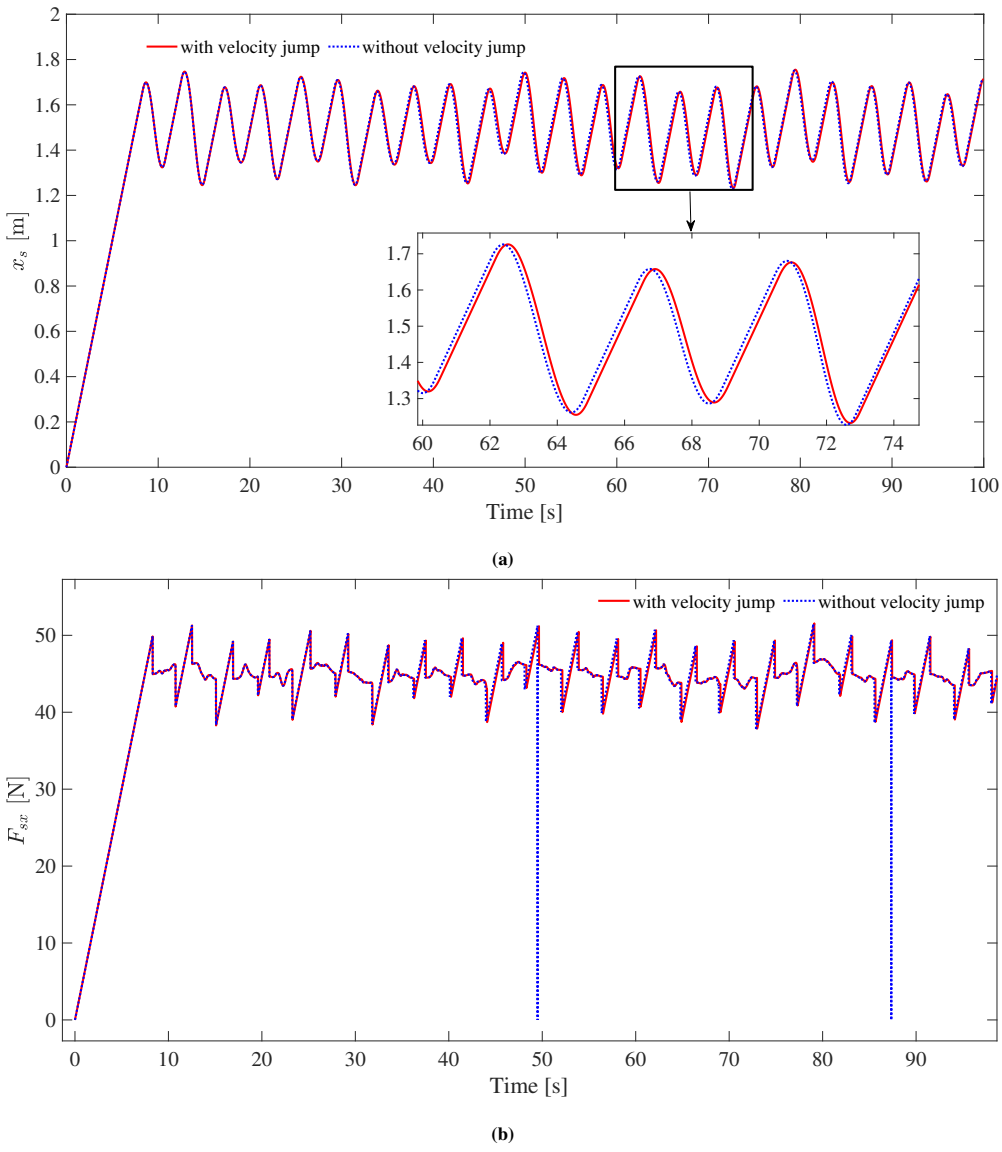

Fig. 6. The impact of velocity jump on (a) displacement; (b) friction force in the x-direction.

3.1. Quantities of interest (QoI)

In order to illustrate the influence of COF random field modelling on the dynamic responses of the system under investigation, dynamic simulations are performed on both the deterministic and stochastic baseline models using the parameters presented in Table.1. Figure 9 collects the results of the time-displacement, time-friction force, and time-velocity (all in the x-direction) plots from the deterministic model and a single long realisation of the stochastic model. Apparent periodic behaviour can be observed from the dynamic displacement and friction force responses of the deterministic model, and the Peak-to-Valley values (PV) of the displacement Δx_d and that of friction force ΔF_d do not change during the entire simulation. In contrast, PVs of the displacement Δx_s and friction force ΔF_{sx} of the stochastic model show strong fluctuations during the simulation. Therefore, Δx_s and ΔF_{sx} can be adopted as two quantities of interest to characterise the difference induced by a random field modelling of COF.

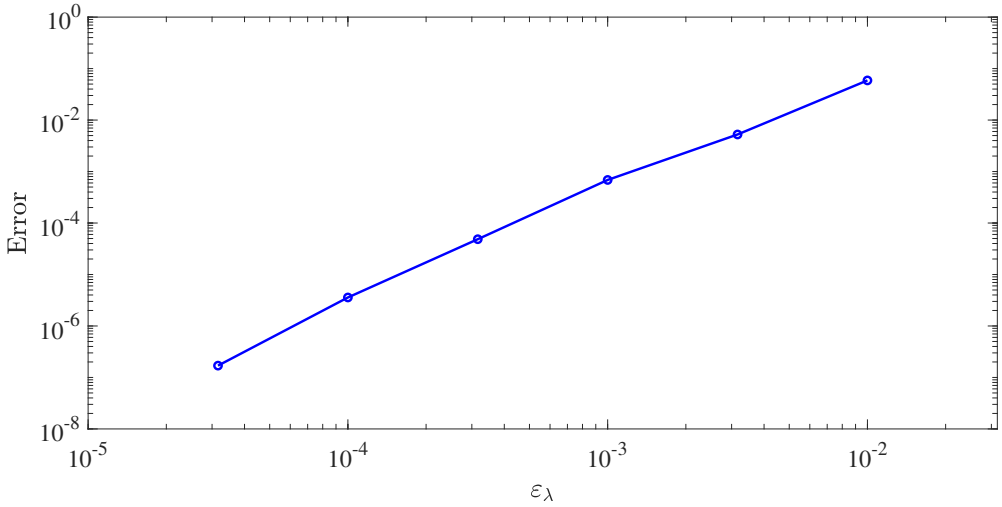

Fig. 7. Error analysis with respect to ε_λ.

Another quantity of interest is the time duration of the stick state t_{stk}. It is of great concern in some industrial contexts. For example, in drilling engineering, a long period in stick state degrades the drilling performance [22]. As can be observed in Fig.9 (e)(f), when the velocity of the disc remains the same as at the belt velocity (in this case $v_b = 0.2\,[m/s]$), the disc is in the stick state. The nondimensionalised time duration of the stick state, represented by the sum of all time spans of the stick state being divided by the total simulation time $T_{sk} = t_{sk}/t_{tot}$, is an intuitive indicator to reveal how the random modelling of COF impacts on the stick-slip motion of the system. In the subsequent sections, a subscript (or superscript) 's' or 'd' means that the quantity is obtained from the stochastic or deterministic model.

3.2. Varying correlation length.

Hereinafter, uncertainties in the QoI of the stochastic model are quantified by varying the correlation length of the baseline model while keeping other parameters unchanged. The correlation length is one of the most important parameters in describing a random field since it determines to what extent randomness is distributed spatially, as shown in Fig.3. With this in mind, the impact of the correlation length on the QoI is analysed by Monte Carlo method with 100 realisations. The total simulation time of each realisation is set to 100 [s], and the initial time step size is set to 10^{-3}s (may vary for the use of bisection method). The threshold ε_λ is set to 10^{-3}. The authors would like to note that since the motion of the disc is quasi-periodic in a single realisation, a number of realisations for a QoI (such as Δx_s) can be collected both inside a single realisation and across realisations using the ergodicity property of the response. A convergence check is performed as shown in Fig.10, where the mean value of $\Delta x_s/\Delta x_d$ converges when the number of realisations exceeds 100.

The outputs of these simulations are collected into three figures in dimensionless forms, as shown in Fig.11, with the horizontal coordinate being nondimensionalised by the characterised length (radius R) of the disc and the vertical coordinate being nondimensionalised by the output of the corresponding deterministic model. It can be observed from

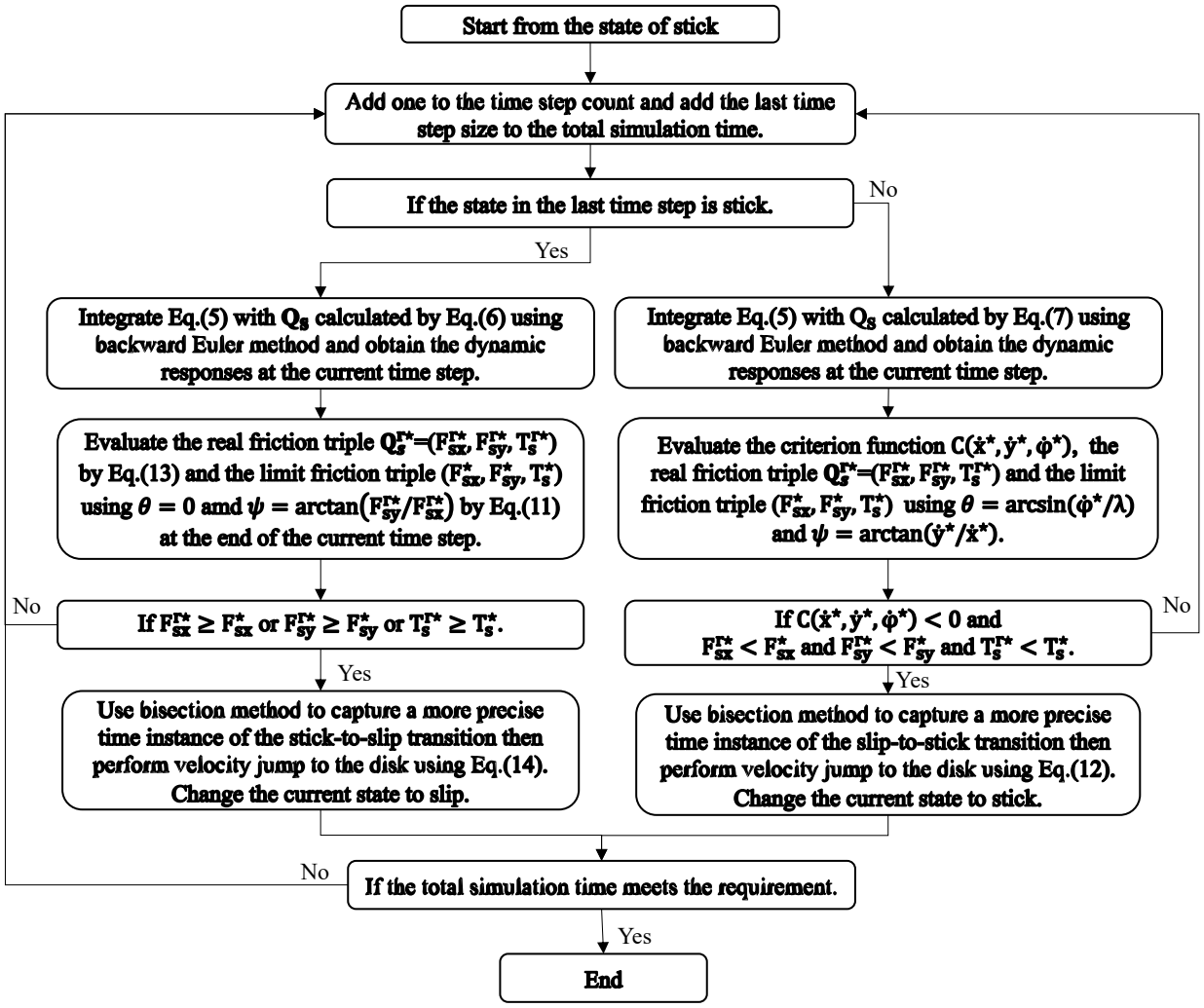

Fig. 8. The flowchart of the algorithm.

Fig.11(a)(b) that correlation length has a significant impact on the PV of the displacement and friction force, both of which share similar patterns. Specifically, the mean value of the stochastic model tends to asymptotically approach that of the deterministic model with an asymptotically vanishing standard deviation when the correlation length is small (e.g. $l/R < 10^{-1}$). On the other side, when l/R increases to be of the order 10^0, the mean value fluctuates strongly around one and the standard deviation surges to its peak value. Finally, when the correlation length becomes so large as $l/R > 10^2$, both the mean value and the standard deviation tend to stabilise at a constant value, where the mean value is slightly lower than one. In Fig.11(c), the observation of the two extreme cases is still applicable: the mean value of the stick duration approaches to one with vanishing standard deviation when $l/R < 10^{-1}$ and become stabilised with constant standard deviation when $l/R > 10^2$. Moreover, the time duration of stick fluctuates the most when l/R is between 10^{-1} and 10^1, where the mean value bends downward from one.

The mechanisms behind these phenomena can be interpreted as follows. When the correlation length becomes very small compared with the characterised length of the disc, the COF of the contact interface takes such a realisation that

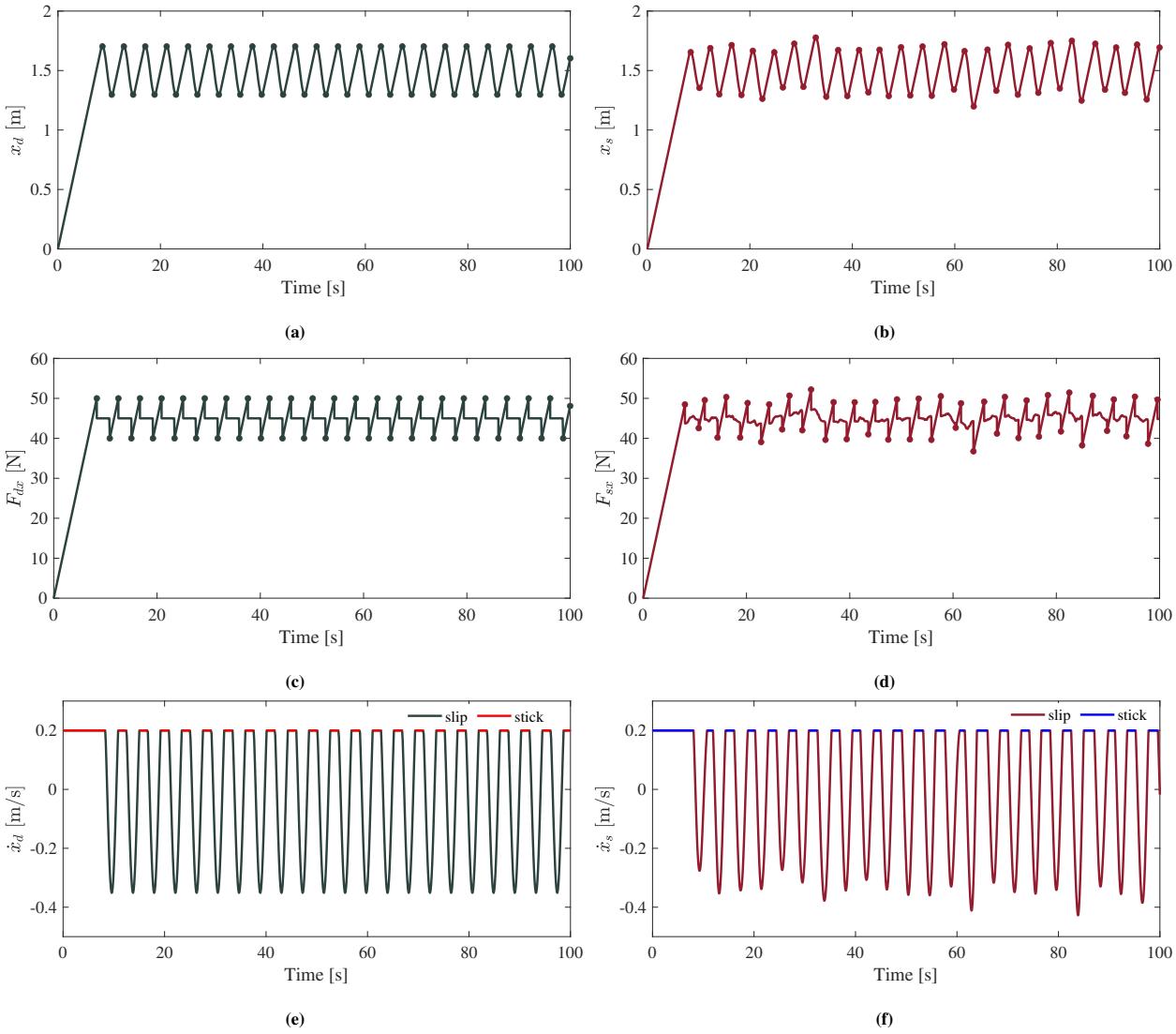

Fig. 9. (a)(c)(e) Dynamic responses of the deterministic baseline model; (b)(d)(f) dynamic responses of the stochastic baseline model.

a large part of the probability distribution can be covered and no significant difference takes place when the contact interface changes due to relative motions between the disc and the belt. In this case, the COF random field of the contact interface can be regarded as a homogenised one equivalent to a deterministic model with its COF being the mean value of the stochastic COF [29]. When the correlation length becomes very large, the COF random field tends to be spatially uniform, of which the random field is comparable to a random variable (with the prescribed mean value and standard deviation of the random field). It also explains that when $l/R > 10^2$, the standard deviations of QoI converge to 0.2, which corresponds to the prescribed coefficient of variation of the COF random field. The inherent stochastic properties of the random field are most prominent when the correlation length and the characterised length of the geometry are comparable.

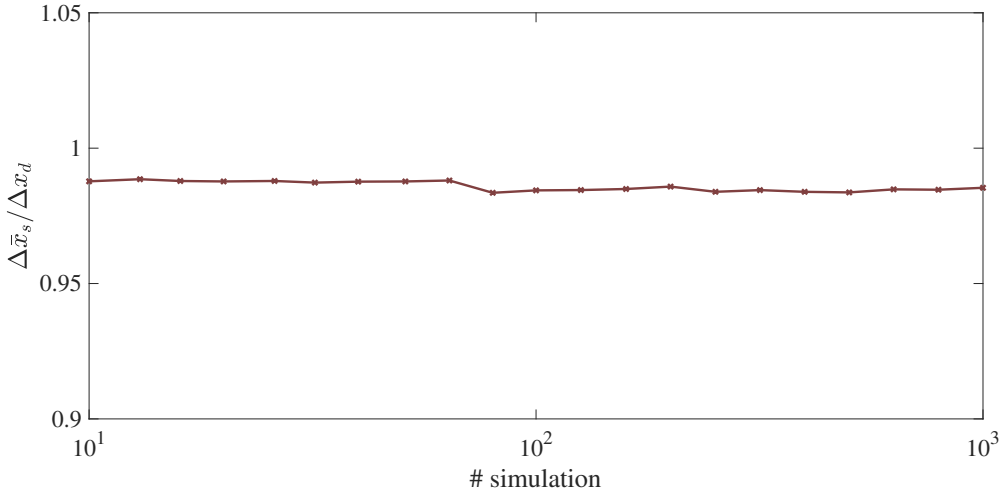

Fig. 10. Nondimensionalised PV of displacement in the x-direction with simulation number

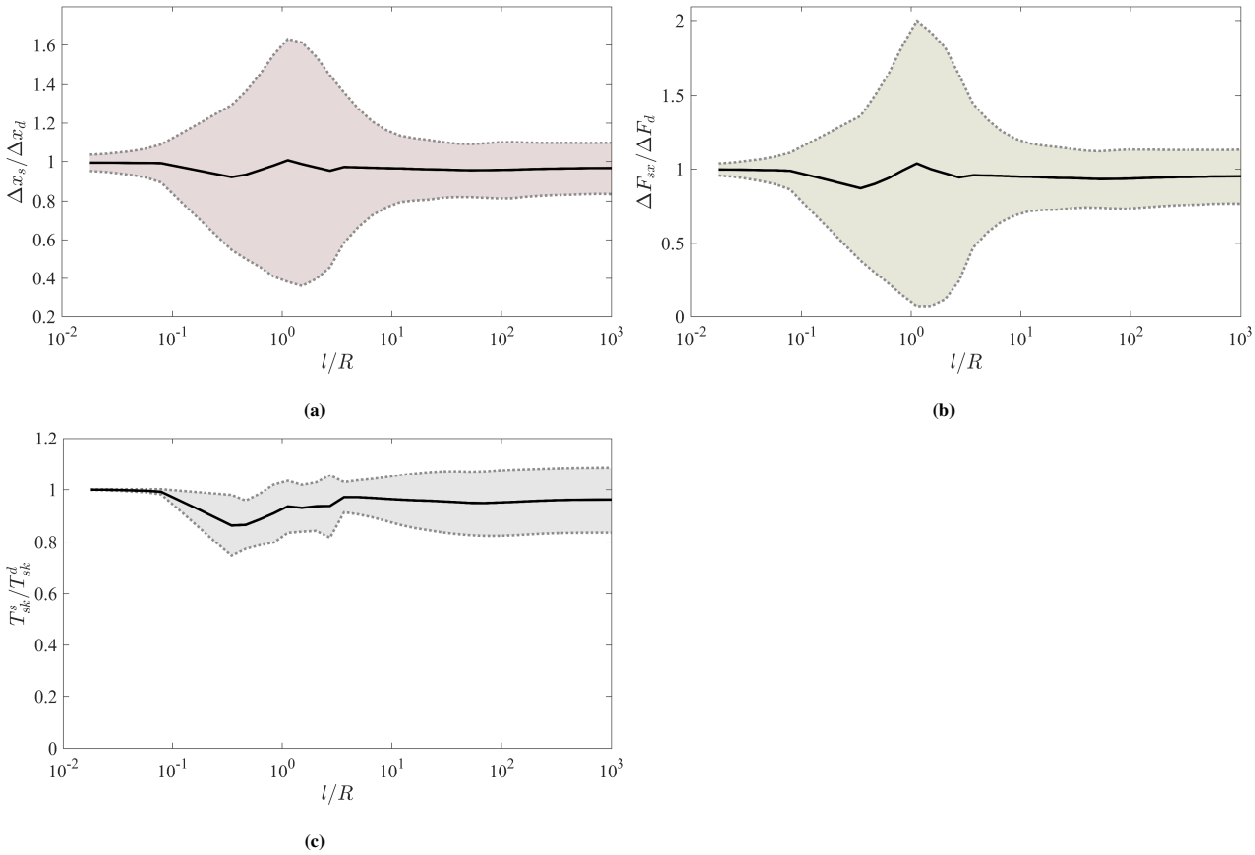

Fig. 11. Stochastic analysis on (a) nondimensionlised PV of displacement in the x-direction; (b) nondimensionlised PV of friction force in the x-direction; (c) nondimensionalised time duration of stick state concerning nondimensionalised varying correlation length of the COF random field. Solid line - mean value; shaded area - standard deviation.

3.3. Varying the belt velocity.

The belt velocity stands as another important parameter since it affects the occurrence of the stick-slip motion of the system. If the belt moves slowly, the disc may soon catch up with the belt and enter into the state of stick. However, if the belt moves fast, the disc may take longer to accelerate to the belt velocity and a shorter stick duration is expected. This section reports stochastic analysis by varying the belt velocity with other parameters equal to the values set for the stochastic baseline model. Other parameters for the numerical solution procedure are the same as described in Sec.3.2.

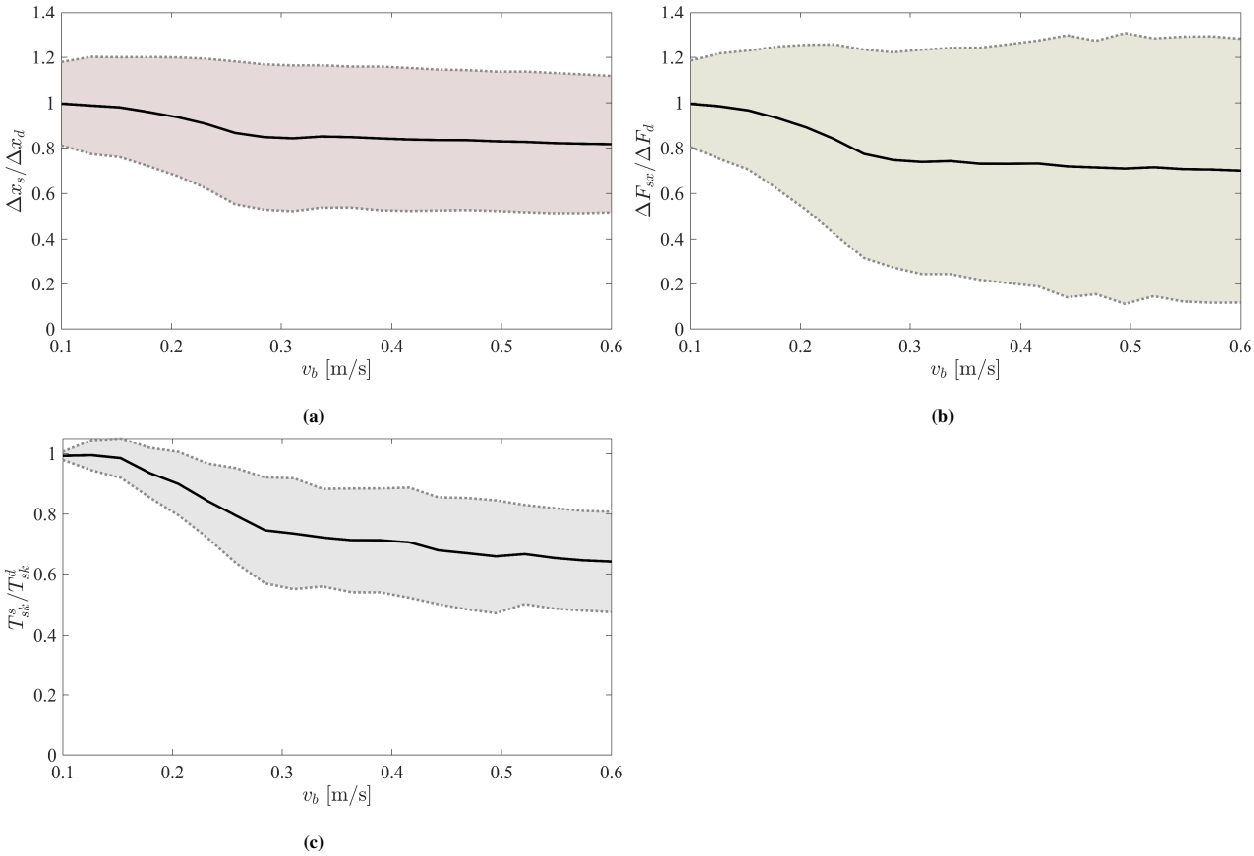

Fig. 12. Stochastic analysis on (a) nondimensionalised PV of displacement in x direction; (b) nondimensionalised PV of friction force in x direction; (c) nondimensionalised time duration of stick state concerning varying the belt velocity. Solid line - mean value; shaded area - standard deviation.

The simulation results are depicted in Fig.12. An immediate observation from these figures is that when the belt velocity increases, all QoI are negatively impacted in the mean sense. The mean value for the PV of the displacement and friction force drops by around 20% in the velocity span under concern. However, the mean value of the stick duration drops by around 40% at $v_b = 0.6$ compared with its value at $v_b = 0.1$. These results demonstrate that the duration of the stick state is tightly connected to the belt velocity. The authors would like to note that although a decrease of the stick duration with an increasing belt velocity for the deterministic model is expected, these results show that the stochasticity would exacerbate this effect, i.e. the stick duration would drop faster because of the introduced randomness in COF. Furthermore, the variation of PV of the displacement increases slightly with the

increase of the belt velocity, while that of the friction force expands massively when the belt velocity grows. This variation expansion indicates that the statistical fluctuations in the friction force become significant in the case of a relatively large belt velocity.

3.4. Varying the mean value of the COF random field.

As a final case of this section, the influence of the mean value of the COF random field is of concern. Specifically, $\mu_{\mathbb{H}_s}$ is varied inside the interval $[0.2, 1]$ with $\sigma_{\mathbb{H}_s}$ determined by a fixed coefficient of variation (CV) as $\mathrm{CV}_{\mathbb{H}_s} = \sigma_{\mathbb{H}_s}/\mu_{\mathbb{H}_s} = 0.2$. The outcomes of the simulation are shown in Fig.13.

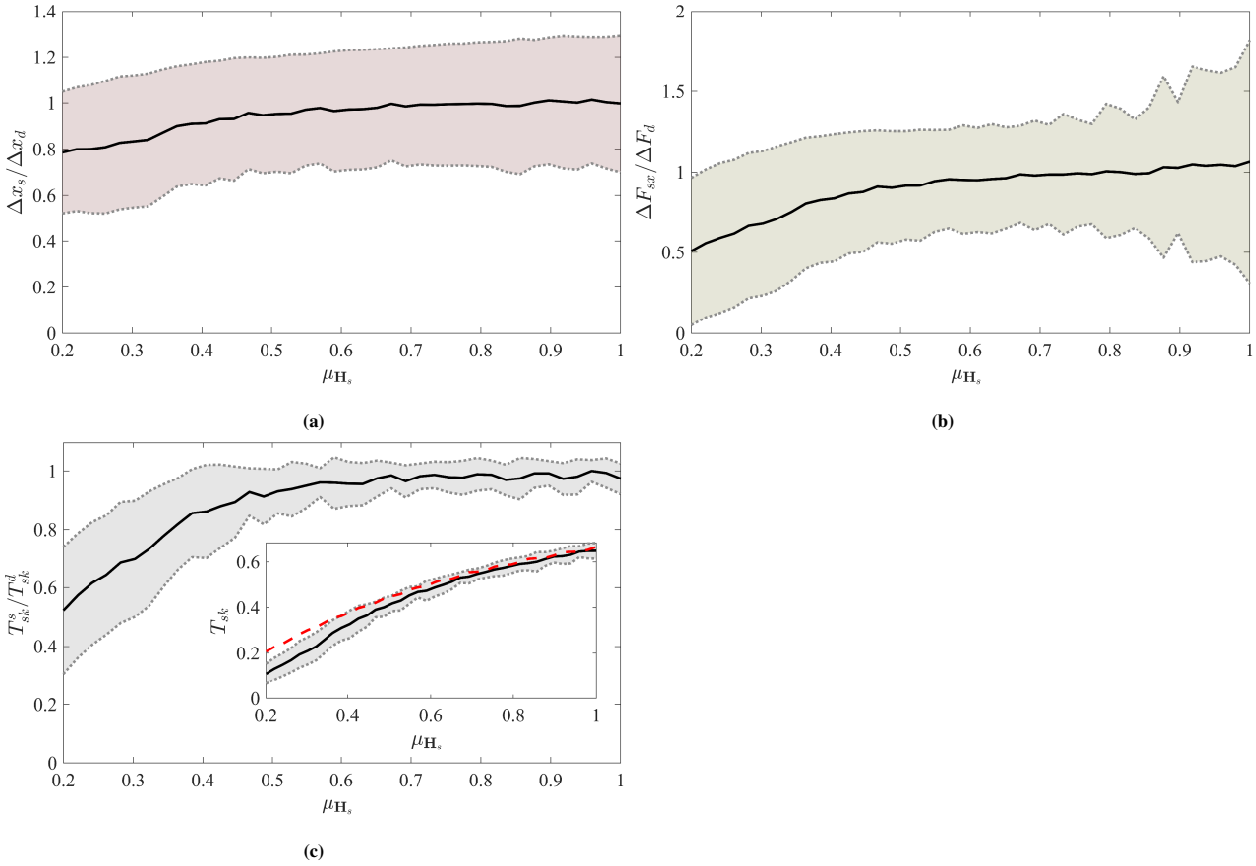

Fig. 13. Stochastic analysis on (a) nondimensionalised PV of displacement in the x-direction; (b) nondimensionalised PV of friction force in the x-direction; (c) nondimensionalised time duration of stick state concerning varying the mean value of the COF random field. The embedded figure presents time duration with dimensions. Dashed line - time duration of stick state of the deterministic model. Solid line - mean value; shaded area - standard deviation.

A first observation of these results is that in contrast to the influence of the belt velocity, increasing $\mu_{\mathbb{H}_s}$ impacts positively all QoI, of which the dimensionless mean values gradually increase and finally saturate at one. The variation of the PV of the displacement remains stable, but that of the friction force increases significantly after $\mu_{\mathbb{H}_s} > 0.8$. In contrast, the variation of the stick duration shrinks with the increase of $\mu_{\mathbb{H}_s}$. These results indicate that, by increasing $\mu_{\mathbb{H}_s}$, the probabilistic expectations of the QoI of the stochastic system turn close to its deterministic counterpart, although variations can be observed in different realisations. The duration of the stick state generally becomes longer if

a larger $\mu_{\mathbb{H}_s}$ is applied, as seen in the embedded figure in Fig.13(c), and the result of the stochastic model approaches asymptotically to that of the deterministic model. Concerning the stick duration aspect, the effect of the spatial fluctuations of the COF become negligible when increasing the mean value of the COF random field.

4. Bifurcation and spectral analysis

After a close inspection of the dynamical properties of the stochastic baseline model shown in Fig.9, apparent non-periodic responses are observed in the x-direction displacement. It is thus natural to look into the phase diagram for more insights. The phase diagrams of both the dynamical responses of the deterministic model and the stochastic model are plotted in Fig.14. The deterministic model and stochastic model results in the x-direction are similar

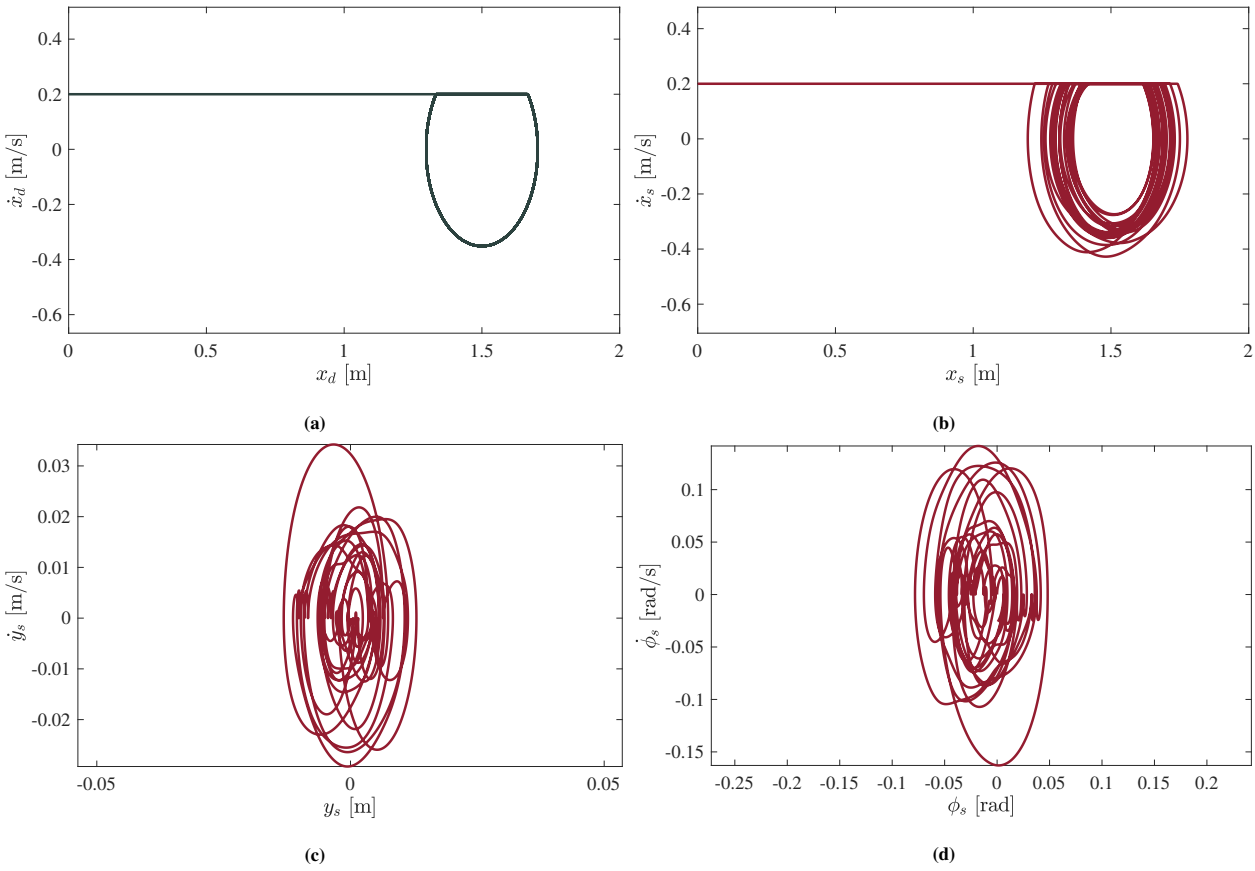

Fig. 14. Phase diagram of the dynamic response of (a) deterministic model; (b) stochastic model in the x-direction; (c) stochastic model in the y-direction; (d) stochastic model in the rotating direction.

concerning the shape of the phase diagrams. For the dynamical response of the deterministic model, its phase diagram only contains a single line and a closed loop, meaning that the motion is utterly periodic except for the initial motion. Additionally, no motion in the y-direction or rotation occurs because of the uniform modelling of the COF in the entire contact interface. On the contrary, phase diagrams of the dynamical responses of the stochastic model exhibit chaotic-like behaviour: the phase diagrams contain multiple irregular loops rather than a finite number of regular

loops, indicating the absence of periodic behaviour. On the other hand, the dynamical responses in the y-direction and rotating direction are similar in the sense that no specific pattern can be found in their phase diagrams since the loops seem to contain significant randomness.

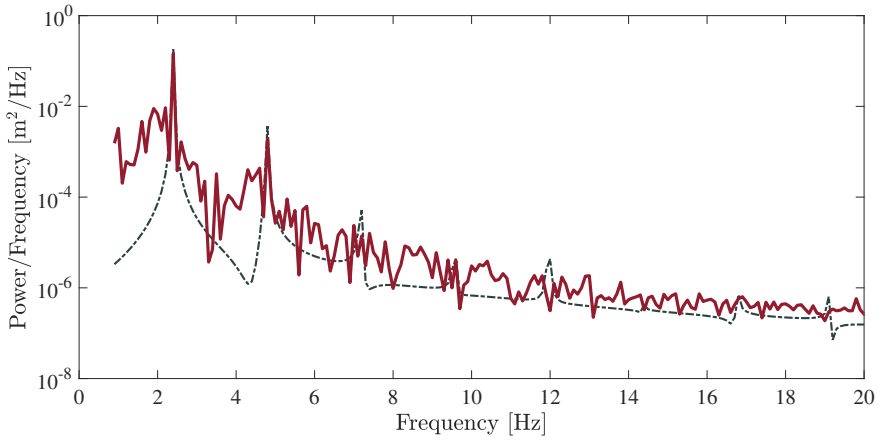

(a)

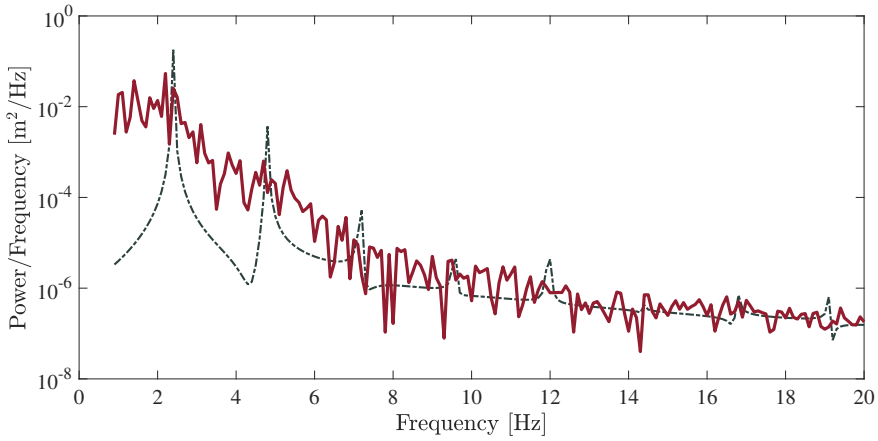

(b)

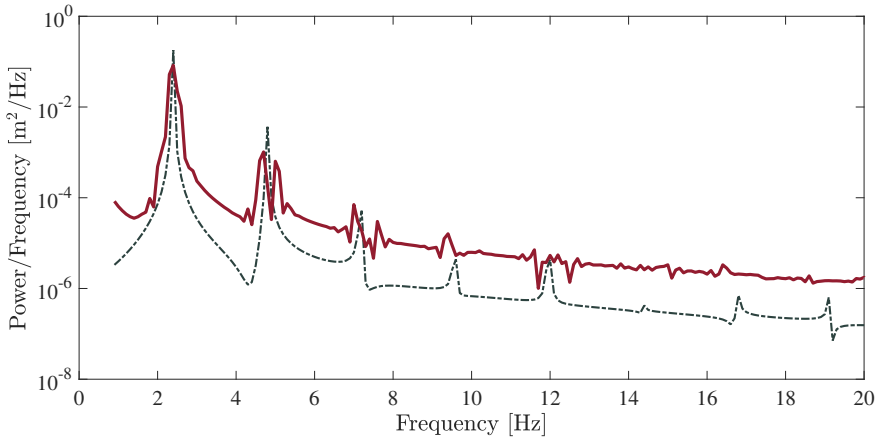

(c)

Fig. 15. Spectrum of the dynamic responses in the x-direction (a) $l/R = 0.1$; (b) $l/R = 1$; (c) $l/R = 10$. Solid line - stochastic model; dashed line - deterministic model.

Spectral analyses of the displacement in the x-direction are also conducted to complement the above analysis. Specifically, three cases where $l/R = 0.1$, $l/R = 1$ and $l/R = 10.0$ are chosen as exemplified analyses. As shown in Fig.15, the peak values of the deterministic model clearly appear at the fundamental frequency and its harmonics, which means the behaviour of the system is periodic without any disturbance. In comparison, the spectrum of the stochastic model, which is obtained using the periodogram method, presents different patterns concerning the nondimensionalised correlation length: (1) for the case where $l/R = 0.1$, shown in Fig.15(a), the spectrum follows approximately the first two peaks of the deterministic model but meanwhile contains a significant amount of noise; (2) for $l/R = 1$ in Fig.15(b), the noise level is enhanced as no meaningful pattern can be observed from the spectrum, which means that even the basic periodicity may not be sustained in a stochastic model; (3) for $l/R = 10.0$ in Fig.15(c), the noise level is substantially reduced, and the first four peaks are found to approximately following those of the deterministic model.

The chaotic-like behaviours found in the dynamic responses of the stochastic model motivate the authors to investigate if the system exhibited certain bifurcation behaviours concerning the variation of model parameters as mentioned in Sec.3. To illustrate the system behaviour, the displacements in the x-direction are recorded at time instants when the disc changes its state from slip to stick. The procedure to conduct simulations is the same as described in Sec.3, except that no repeated realisations using the same parameters are needed because the statistical properties of the output are out of concern in this case. These results are presented in Fig.16. It is again observed that the nondimensionalised correlation length significantly affects the system responses: when $l/R < 10^{-1}$, the system has only one steady state and the responses look much like a deterministic one; when $10^0 < l/R < 10^1$, the results are significantly dispersed, showing that no steady state exists; however, multiple steady states can be found when $l/R > 10^2$ for the data recorded forms several separable clusters. Conversely, the impact of the belt velocity is believed not to be prominent upon the bifurcation behaviour of the system, as seen in Fig.16(b), and the recorded data is scattered at approximately the same level for the variation of the belt velocity. On the other side, the mean value of the static COF shows a positive influence on the dispersion of the results when increasing its value. As a comparison, the data recorded from the deterministic model results shows that the system is always in a steady state in all three cases above.

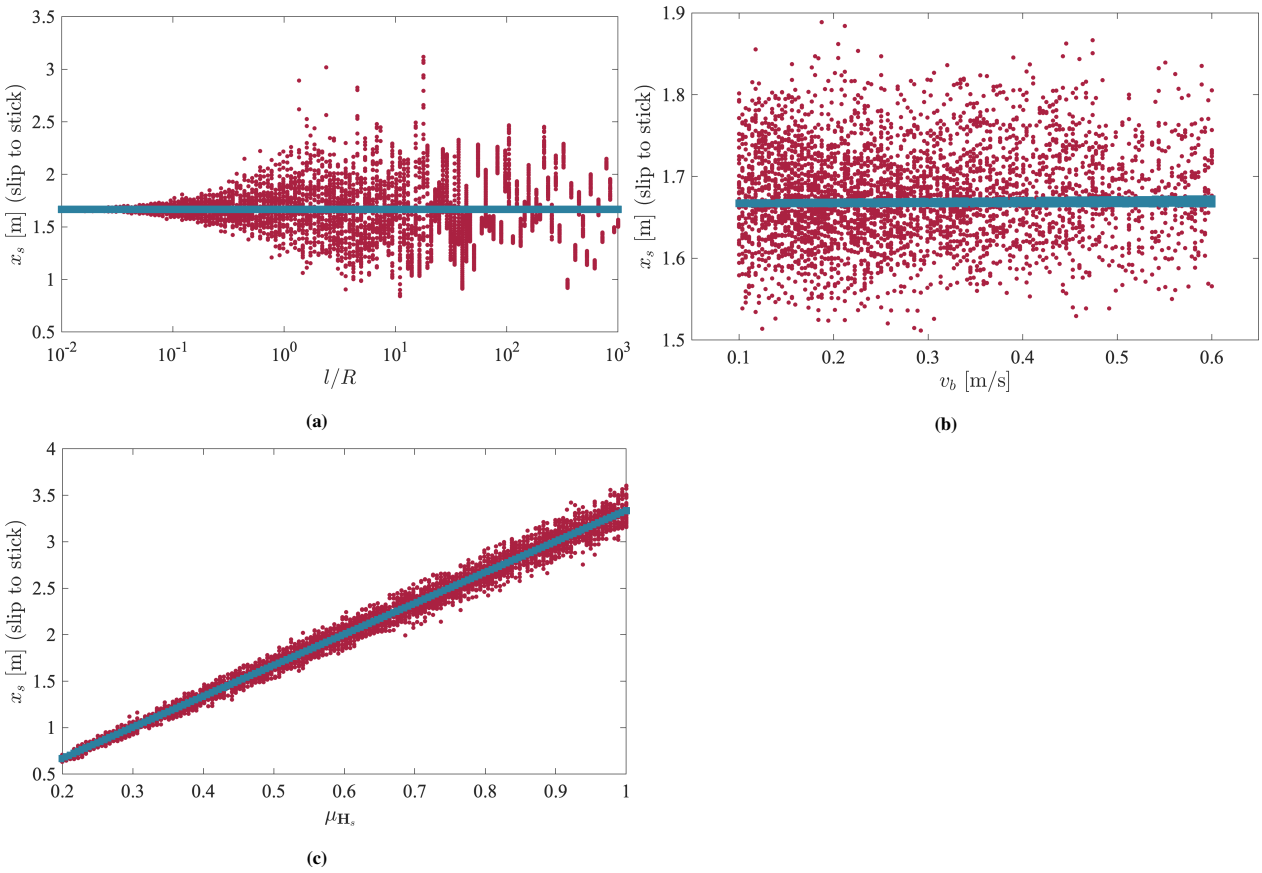

Fig. 16. Bifurcation behaviours of the stochastic model concerning (a) the correlation length of the COF random field; (b) the belt velocity; (c) the mean value of the COF random field. Dot marker - data from stochastic model; square marker - data from deterministic model.

5. Conclusions

In this paper, the stick-slip motion of a slider-on-belt model is investigated with the contact interface modelled as a random field. For this purpose, a lognormal random field is generated by the circulant embedding method and Nataf transform. New three-variable stick-slip criteria are then proposed to capture an accurate transition point from the state of stick to slip, or *vice versa*. The new method proposed in this paper is then used to establish new findings. Stochastic and bifurcation analyses are conducted to reveal the inherent properties of the slider-on-belt model with respect to three crucial system properties: the nondimesionalised correlation length l/R, the belt velocity v_b and the mean value of the COF random field $\mu_{\mathbb{H}_s}$.

The results of these analyses can be summarised as follows. (1) l/R is found to be dominantly responsible for the stochastic responses of the system. When $l/R < 10^{-1}$, the stochastic model degenerates to a deterministic one due to homogenisation effects; When $l/R > 10^{2}$, the COF random field reduces to a random variable as the field becomes spatially uniform but is statistically random. In this case, the random field can be replaced by a random variable, making the analysis easier to conduct. When l/R takes value in between, the system exhibits prominent stochastic behaviour (e.g. large variation of displacement and friction force), and the effect of COF random field

modelling should be taken into account. (2) Belt velocity is a deterministic parameter in this work, but it can amplify the uncertainties in the displacement and friction force and reduce the time duration of stick state compared with the deterministic model when v_b increases. (3) An increasing mean value of the static COF tends to make the dynamical responses of the stochastic model approach closely its deterministic counterpart. However, uncertainties still exist as being amplified in the friction force but reduced in the time duration of the stick state.

Acknowledgment

The first author H. Hu gratefully acknowledges the financial support from the University of Liverpool and China Scholarship Council Awards (CSC NO.201906230311).

Appendix A Random field generation: the circulant embedding method

This appendix presents an algorithm for generating a two-dimensional normalised homogeneous Gaussian random field using the circulant embedding method. For more details, please refer to [45, 46]. Consider the generation of a normalised homogeneous Gaussian random field with correlation function shown as Eq.(2) over a rectangular domain as $\mathcal{D}$ of $m \times n$ grid points $\mathcal{D} = \{(i\Delta x, j\Delta y), i = 0, \ldots, m-1, j = 0, \ldots, n-1\}$. The algorithm can be summarised into the following steps:

(1) **Constructing the covariance matrix.** Rearrange the grid points into a column vector $\mathbf{g}$ of size mn and the covariance matrix $\mathbf{\Sigma}$ of size $mn \times mn$ can be generated with component

$$\begin{aligned} \Sigma_{i,j} = \mathrm{Cov}(x_i - x_j, y_i - y_j) &= \sigma^2 \mathrm{R}_{\mathbb{H}}(x_i - x_j, y_i - y_j), \\ x_i - x_j &= [\mathrm{mod}(i-1, m) - \mathrm{mod}(j-1, m)]\Delta x, \\ y_i - y_j &= (\lceil i/m \rceil - \lceil j/m \rceil)\Delta y, \end{aligned} \tag{A.1}$$

where $\sigma = 1$ is the standard deviation for a normalised Gaussian distribution and $\lceil \cdot \rceil$ indicates approximating to a ceiling number. In this case, matrix $\mathbf{\Sigma}$ becomes a block-Toeplitz matrix with each block of size $m \times m$ itself a Toeplitz matrix. Therefore, as Σ is also symmetric, it can be completely characterised by its first block row $\mathbf{B} = (\mathbf{B_1}, \mathbf{B_2}, \ldots, \mathbf{B_n})$.

(2) **Embedding in block circulant matrix.** The purpose is that by embedding $\mathbf{B}$ into a square circulant matrix $\mathbf{S}$, the eigenvalue decomposition can be derived, which is essential to form a realisation of the random field, as will be seen in subsequent steps. Firstly, each block matrix $\mathbf{B_i}$ is extended to a circulant matrix $\mathbf{C_i}$ of size $(2m-1) \times (2m-1)$. Then the first block row of $\mathbf{S}$ can be obtained in the sense of minimal embedding as $\mathbf{C} = (\mathbf{C_1}, \ldots, \mathbf{C_n}, \mathbf{C_2^T}, \ldots, \mathbf{C_n^T})$, which results in $\mathbf{S}$ being of the size $M \times M$, where $M = (2m-1)(2n-1)$. Finally, $\mathbf{S}$ is completely characterised by its first block row as it is also block-circulant.

(3) **Eigendecomposition.** It is known that a circulant matrix can be diagonalised as $\mathbf{S} = 1/M\mathbf{F}\mathbf{\Lambda}\mathbf{F}^\star$ and $\mathbf{F}$ is the two-dimensional discrete Fourier transform matrix of size $M \times M$ [49]. $\mathbf{F}^\star$ is the conjugate transpose of $\mathbf{F}$, and $\mathbf{\Lambda}$ is a diagonal eigenvalue matrix of size $M \times M$ whose diagonal entries form the vector $\boldsymbol{\gamma} = \mathbf{Fs}$, where $\mathbf{s}$ is a vector containing the transpose of entries in the first row of $\mathbf{S}$, and this calculation can be accelerated by FFT technique.

(4) **Gaussian random field realisation.** The circulant matrix $\mathbf{S}$ has decomposition as $\mathbf{S} = \mathbf{F}\mathbf{\Lambda}^{\frac{1}{2}}(\mathbf{F}\mathbf{\Lambda}^{\frac{1}{2}})^{\star}$ provided that all components in $\boldsymbol{\gamma}$ are nonnegative. If the semi-positive definite condition of $\mathbf{S}$ is satisfied, a random field can be realised by taking either the real or imaginary part of the vector $\mathbf{\Gamma} = \mathbf{F}(\mathbf{\Lambda}/M)^{\frac{1}{2}}\boldsymbol{\xi}$, where $\boldsymbol{\xi} = \boldsymbol{\xi}_1 + \mathrm{i}\boldsymbol{\xi}_2$ is a complex random vector of dimension M with $\boldsymbol{\xi}_1$ and $\boldsymbol{\xi}_2$ being two normal random variables of zero mean and identity covariance matrix. As in step (3), this calculation can be done via FFT. The random field vector $\mathbf{\Gamma}$, corresponding to the grid point vector $\mathbf{g}$, has an expected distribution as $\mathcal{N}(\mathbf{0}, \mathbf{\Sigma})$.

References

[1] K. Popp, P. Stelter, Stick-slip vibrations and chaos, Philosophical Transactions: Physical Sciences and Engineering (1990) 89–105doi:http://www.jstor.org/stable/76822.

[2] H. Ouyang, W. Nack, Y. Yuan, F. Chen, Numerical analysis of automotive disc brake squeal: a review, International Journal of Vehicle Noise and Vibration 1 (3-4) (2005) 207–231. doi:http://dx.doi.org/10.1504/IJVNV.2005.007524.

[3] B. Feeny, A. s. Guran, N. Hinrichs, K. Popp, A historical review on dry friction and stick-slip phenomena, Applied Mechanics Reviews 51 (5) (1998) 321–341. doi:10.1115/1.3099008.

[4] W. Brace, J. Byerlee, Stick-slip as a mechanism for earthquakes, Science 153 (3739) (1966) 990–992. doi:http://dx.doi.org/10.1126/science.153.3739.990.

[5] T. Kousaka, H. Asahara, N. Inaba, Stick-slip chaos in a mechanical oscillator with dry friction, Progress of Theoretical and Experimental Physics 2018 (3) (2018) 033A01. doi:http://dx.doi.org/10.1093/ptep/pty016.

[6] Z. Du, H. Fang, X. Zhan, J. Xu, Experiments on vibration-driven stick-slip locomotion: a sliding bifurcation perspective, Mechanical Systems and Signal Processing 105 (2018) 261–275. doi:http://dx.doi.org/10.1016/j.ymssp.2017.12.001.

[7] R. Leine, D. Van Campen, A. De Kraker, L. Van Den Steen, Stick-slip vibrations induced by alternate friction models, Nonlinear dynamics 16 (1) (1998) 41–54. doi:https://doi.org/10.1023/A:1008289604683.

[8] A. C. LUO, B. C. GEGG, On the mechanism of stick and nonstick, periodic motions in a periodically forced, linear oscillator with dry friction, Journal of vibration and acoustics 128 (1) (2006) 97–105. doi:http://dx.doi.org/10.1126/science.153.3739.990.

[9] A. C. Luo, B. C. Gegg, Stick and non-stick periodic motions in periodically forced oscillators with dry friction, Journal of Sound and Vibration 291 (1) (2006) 132–168. doi:https://doi.org/10.1016/j.jsv.2005.06.003.

[10] C. Dong, J. Mo, C. Yuan, X. Bai, Y. Tian, Vibration and noise behaviors during stick–slip friction, Tribology Letters 67 (4) (2019) 1–12. doi:http://dx.doi.org/10.1007/s11249-019-1216-1.

[11] N. Liu, H. Ouyang, Friction-induced vibration of a slider-on-rotating-disc system considering uniform and non-uniform friction characteristics with bi-stability, Mechanical Systems and Signal Processing 164 (2022) 108222. doi:https://doi.org/10.1016/j.ymssp.2021.108222.

[12] Z. Li, H. Ouyang, Z. Guan, Friction-induced vibration of an elastic disc and a moving slider with separation and reattachment, Nonlinear Dynamics 87 (2) (2017) 1045–1067. doi:http://dx.doi.org/10.1007/s11071-016-3097-2.

[13] Z. Li, Q. Cao, Z. Nie, Stick-slip vibrations of a self-excited sd oscillator with coulomb friction, Nonlinear Dynamics 102 (3) (2020) 1419–1435. doi:http://dx.doi.org/10.1007/s11071-020-06009-3.

[14] X. Wang, B. Huang, R. Wang, J. Mo, H. Ouyang, Friction-induced stick-slip vibration and its experimental validation, Mechanical Systems and Signal Processing 142 (2020) 106705. doi:http://dx.doi.org/10.1016/j.ymssp.2020.106705.

[15] U. J. F. Aarsnes, F. Di Meglio, R. J. Shor, Avoiding stick slip vibrations in drilling through startup trajectory design, Journal of Process Control 70 (2018) 24–35. doi:http://dx.doi.org/10.1016/j.jprocont.2018.07.019.

[16] L. Hong, I. P. Girsang, J. S. Dhupia, Identification and control of stick–slip vibrations using kalman estimator in oil-well drill strings, Journal of Petroleum Science and Engineering 140 (2016) 119–127. doi:http://dx.doi.org/10.1016/j.petrol.2016.01.017.

[17] X. Zheng, V. Agarwal, X. Liu, B. Balachandran, Nonlinear instabilities and control of drill-string stick-slip vibrations with consideration of state-dependent delay, Journal of Sound and Vibration 473 (2020) 115235. doi:http://dx.doi.org/10.1016/j.jsv.2020.115235.

[18] F. Marques, P. Flores, J. P. Claro, H. M. Lankarani, A survey and comparison of several friction force models for dynamic analysis of multibody mechanical systems, Nonlinear Dynamics 86 (3) (2016) 1407–1443. doi:http://dx.doi.org/10.1007/s11071-016-2999-3.

[19] Q. Feng, A discrete model of a stochastic friction system, Computer methods in applied mechanics and engineering 192 (20-21) (2003) 2339–2354. doi:http://dx.doi.org/10.1016/S0045-7825(03)00241-X.

[20] O. Ben-David, J. Fineberg, Static friction coefficient is not a material constant, Physical review letters 106 (25) (2011) 254301. doi:http://dx.doi.org/10.1103/PhysRevLett.106.254301.

[21] F. Chen, M. K. Abdelhamid, P. Blaschke, J. Swayze, On automotive disc brake squeal part iii test and evaluation, Tech. rep., SAE Technical Paper (2003). doi:http://dx.doi.org/10.4271/2003-01-1622.

[22] R. Lima, R. Sampaio, Stick-mode duration of a dry-friction oscillator with an uncertain model, Journal of Sound and Vibration 353 (2015) 259–271. doi:http://dx.doi.org/10.1016/j.jsv.2015.05.015.

[23] R. Lima, R. Sampaio, Construction of a statistical model for the dynamics of a base-driven stick-slip oscillator, Mechanical Systems and Signal Processing 91 (2017) 157–166. doi:http://dx.doi.org/10.1016/j.ymssp.2016.12.038.

[24] H. Qiu, J. Yang, S. Butt, Investigation on bit stick-slip vibration with random friction coefficients, Journal of Petroleum Science and Engineering 164 (2018) 127–139. doi:http://dx.doi.org/10.1016/j.petrol.2018.01.037.

[25] A. Lima, C. F. Moukarzel, I. Grosse, T. Penna, Sliding blocks with random friction and absorbing random walks, Physical Review E 61 (3) (2000) 2267. doi:http://dx.doi.org/10.1103/PhysRevE.61.2267.

[26] R. Murthy, B.-K. Choi, X. Wang, M. C. Sipperley, M. P. Mignolet, C. Soize, Maximum entropy modeling of discrete uncertain properties with application to friction, Probabilistic Engineering Mechanics 44 (2016) 128–137. doi:http://dx.doi.org/10.1016/j.probengmech.2015.10.003.

[27] B.-K. Choi, M. Sipperley, M. Mignolet, C. Soize, Discrete maximum entropy process modeling of uncertain properties: Application to friction for stick-slip and microslip response, 2011, pp. 2626–2633.
URL https://hal-upec-upem.archives-ouvertes.fr/hal-00693053

[28] T. Ritto, M. Escalante, R. Sampaio, M. B. Rosales, Drill-string horizontal dynamics with uncertainty on the frictional force, Journal of Sound and Vibration 332 (1) (2013) 145–153. doi:http://dx.doi.org/10.1016/j.jsv.2012.08.007.

[29] H. Hu, A. Batou, H. Ouyang, Coefficient of friction random field modelling and analysis in planar sliding, Journal of Sound and Vibration (2021) 116197doi:10.1016/j.jsv.2021.116197.

[30] J. Barber, X. Wang, Numerical algorithms for two-dimensional dynamic frictional problems, Tribology International 80 (2014) 141–146. doi:http://dx.doi.org/10.1016/j.triboint.2014.07.004.

[31] F. A. Tariku, R. J. Rogers, Improved dynamic friction models for simulation of one-dimensional and two-dimensional stick-slip motion, J. Trib. 123 (4) (2001) 661–669. doi:http://dx.doi.org/10.1115/1.1331057.

[32] M. Fadaee, S. Yu, Two-dimensional stick-slip motion of coulomb friction oscillators, Proceedings of the Institution of Mechanical Engineers, Part C: Journal of Mechanical Engineering Science 230 (14) (2016) 2438–2448. doi:http://dx.doi.org/10.1177/0954406215597954.

[33] F. Xia, Modelling of a two-dimensional coulomb friction oscillator, Journal of Sound and Vibration 265 (5) (2003) 1063–1074. doi:http://dx.doi.org/10.1016/S0022-460X(02)01444-X.

[34] I. Kardan, M. Kabganian, R. Abiri, M. Bagheri, Stick-slip conditions in the general motion of a planar rigid body, Journal of Mechanical Science and Technology 27 (9) (2013) 2577–2583. doi:http://dx.doi.org/10.1007/s12206-013-0701-y.

[35] G. Kudra, J. Awrejcewicz, Bifurcational dynamics of a two-dimensional stick-slip system, Differential Equations and Dynamical Systems 20 (3) (2012) 301–322. doi:https://doi.org/10.1007/s12591-012-0104-z.

[36] G. Kudra, J. Awrejcewicz, A smooth model of the resultant friction force on a plane contact area, Journal of Theoretical and Applied Mechanics 54 (3) (2016) 909–919. doi:http://dx.doi.org/10.15632/jtam-pl.54.3.909.

[37] P. Abrahamsen, A review of Gaussian random fields and correlation functions, Norsk Regnesentral/Norwegian Computing Center (1997) 64doi:10.13140/RG.2.2.23937.20325.

[38] G. Matheron, The intrinsic random functions and their applications, Advances in applied probability 5 (3) (1973) 439–468. doi:http://dx.doi.org/10.2307/1425829.

[39] A. Mantoglou, J. L. Wilson, The turning bands method for simulation of random fields using line generation by a spectral method, Water Resources Research 18 (5) (1982) 1379–1394. doi:http://dx.doi.org/10.1029/WR018i005p01379.

[40] M. Shinozuka, Simulation of multivariate and multidimensional random processes, The Journal of the Acoustical Society of America 49 (1B) (1971) 357–368. doi:http://dx.doi.org/10.1121/1.1912338.

[41] M. Shinozuka, G. Deodatis, Simulation of multi-dimensional Gaussian stochastic fields by spectral representation, Applied Mechanics Reviews 49 (1996) 29–53. doi:http://dx.doi.org/10.1115/1.3101883.

[42] M. W. Davis, Production of conditional simulations via the lu triangular decomposition of the covariance matrix, Mathematical Geology 19 (1987) 91–98. doi:https://doi.org/10.1007/BF00898189.

[43] R. Ghanem, P. Spanos, Stochastic finite elements: A spectral approach, 1990. doi:http://dx.doi.org/10.1007/978-1-4612-3094-6.

[44] Y. Liu, J. Li, S. Sun, B. Yu, Advances in Gaussian random field generation: a review, Computational Geosciences 23 (5) (2019) 1011–1047. doi:http://dx.doi.org/10.1007/s10596-019-09867-y.

[45] C. R. Dietrich, G. N. Newsam, Fast and exact simulation of stationary Gaussian processes through circulant embedding of the covariance matrix, SIAM Journal on Scientific Computing 18 (4) (1997) 1088–1107. doi:http://dx.doi.org/10.1137/S1064827592240555.

[46] D. P. Kroese, Z. I. Botev, Spatial process simulation, in: Stochastic geometry, spatial statistics and random fields, Springer, 2015, pp. 369–404. doi:http://dx.doi.org/10.1007/978-3-319-10064-7_12.

[47] R. Lebrun, A. Dutfoy, An innovating analysis of the nataf transformation from the copula viewpoint, Probabilistic Engineering Mechanics 24 (3) (2009) 312–320. doi:http://dx.doi.org/10.1016/j.probengmech.2008.08.001.

[48] W. Puła, D. Griffiths, Transformations of spatial correlation lengths in random fields, Computers and Geotechnics 136 (2021) 104151. doi:https://doi.org/10.1016/j.compgeo.2021.104151.

[49] J. C. R. Claeyssen, L. A. dos Santos Leal, Diagonalization and spectral decomposition of factor block circulant matrices, Linear algebra and its applications 99 (1988) 41–61. doi:http://dx.doi.org/10.1016/0024-3795(88)90124-3.